The Plant Cell, Vol. 26: 1480–1496, April 2014, www.plantcell.org

Analysis of the Root System Architecture of *Arabidopsis* Provides a Quantitative Readout of Crosstalk between Nutritional Signals[W][OPEN]

Fabian Kellermeier,[a] Patrick Armengaud,[b] Triona J. Seditas,[a] John Danku,[c] David E. Salt,[c] and Anna Amtmann[a,1]

[a] Institute of Molecular, Cell, and Systems Biology, College of Medical, Veterinary, and Life Sciences, University of Glasgow, Glasgow G12 8QQ, United Kingdom

[b] INRA, UMR1318 INRA-AgroParisTech, Institut Jean-Pierre Bourgin, INRA Centre de Versailles-Grignon, 78026 Versailles, France

[c] Institute of Biological and Environmental Sciences, College of Life Sciences and Medicine, University of Aberdeen, Aberdeen AB24 3UU, United Kingdom

As plant roots forage the soil for food and water, they translate a multifactorial input of environmental stimuli into a multifactorial developmental output that manifests itself as root system architecture (RSA). Our current understanding of the underlying regulatory network is limited because root responses have traditionally been studied separately for individual nutrient deficiencies. In this study, we quantified 13 RSA parameters of *Arabidopsis thaliana* in 32 binary combinations of N, P, K, S, and light. Analysis of variance showed that each RSA parameter was determined by a typical pattern of environmental signals and their interactions. P caused the most important single-nutrient effects, while N-effects were strongly light dependent. Effects of K and S occurred mostly through nutrient interactions in paired or multiple combinations. Several RSA parameters were selected for further analysis through mutant phenotyping, which revealed combinations of transporters, receptors, and kinases acting as signaling modules in K–N interactions. Furthermore, nutrient response profiles of individual RSA features across NPK combinations could be assigned to transcriptionally coregulated clusters of nutrient-responsive genes in the roots and to ionome patterns in the shoots. The obtained data set provides a quantitative basis for understanding how plants integrate multiple nutritional stimuli into complex developmental programs.

INTRODUCTION

Plants alter the growth and development of individual parts of the root system to achieve a root system architecture (RSA) that is best suited to forage the soil for mineral nutrients and water. Adaptation of RSA occurs during evolution (apparent as RSA plasticity among species and ecotypes) and within the life of an individual (apparent as changes of RSA in response to fluctuating nutrient supply), and recent evidence suggests that RSA plasticity at both levels involves the same key regulators (Rosas et al., 2013). Understanding the molecular mechanisms that adapt the root system to nutrient starvation is essential for predicting and improving yield and nutritional quality of plants in the field and on marginal land (Den Herder et al., 2010).

RSA is the net product of differential growth dynamics in different parts of the root (López-Bucio et al., 2003). In dicotyledonous plants, such as *Arabidopsis thaliana*, the root displays a hierarchical tree structure with one primary main root producing lateral roots, which in turn produce higher-order lateral roots. Even this simple basic structure can produce a wealth of architectures by varying the frequency of lateral root emergence and the growth rate of individual root parts (Hodge et al., 2009; De Smet et al., 2012). Analysis of RSA provides an excellent quantitative readout for identifying the genes and signaling pathways that enable plants to perceive changes in the root environment and to integrate them into adaptive responses. However, the multifactorial nature of both input (many environmental stimuli) and output (many individual RSA features) has not been fully captured to date; hence, our understanding of signal integration in plant roots is still rudimentary.

Research on the effects of individual mineral deficiencies on a limited set of RSA parameters has revealed several important components of nutrient signaling pathways. For example, lateral root emergence and elongation in response to nitrate supply requires the nitrate transporter NRT2.1 (Little et al., 2005) and the nitrate transporter/receptor NRT1.1 (Remans et al., 2006), the latter being regulated by the Calcineurin B-Like (CBL)-Interacting Protein Kinase 23 (CIPK23) (Ho et al., 2009), as well as MADS box transcription factor ANR1 (Zhang and Forde, 1998; Gan et al., 2012), ARF8 (a target of microRNA 167; Gifford et al., 2008) and AFB3 (a target of microRNA 393; Vidal et al., 2013). The phytohormone auxin is essential for lateral root emergence, and its reallocation within the root is an important part of the RSA response to nitrate (Krouk et al., 2010). Some studies also report an auxin-dependent increase in lateral root density in low phosphate (López-Bucio et al., 2002; Nacry et al., 2005; Pérez-Torres et al., 2008; Miura et al., 2011), although it has been debated to what extent other environmental factors

[1] Address correspondence to anna.amtmann@glasgow.ac.uk.
The author responsible for distribution of materials integral to the findings presented in this article in accordance with the policy described in the Instructions for Authors (www.plantcell.org) is: Anna Amtmann (anna.amtmann@glasgow.ac.uk).

[W] Online version contains Web-only data.

[OPEN] Articles can be viewed online without a subscription.

www.plantcell.org/cgi/doi/10.1105/tpc.113.122101

contribute to this response (De Smet et al., 2012; Dubrovsky and Forde, 2012). More conspicuously, P starvation inhibits elongation of the main root (Williamson et al., 2001), a root-apex delimited response that involves the multicopper-oxidase LRP1 and the P5-type ATPase PDR2 (Svistoonoff et al., 2007; Ticconi et al., 2009). Main root elongation in low P can be rescued by lowering iron, which suggests interaction between P and Fe signaling (Ward et al., 2008; Abel, 2011).

The traditional view that each individual nutrient deficiency induces an architecture that is typical for the nutrient (López-Bucio et al., 2003) has recently been broadened by the measurement of RSA profiles over a wider concentration range of a given nutrient (Gruber et al., 2013). Further complexity arises from the fact that in the soil several nutrients can be deficient at the same time and in different combinations. To date, the effects of multiple nutrient deficiencies have not been studied systematically. At this stage, we do not know whether RSA responses to individual nutrients are additive under multiple deficiencies, whether certain responses are prioritized over others, or whether each nutrient combination produces entirely new RSAs. In the light of known interactions between carbon and nitrogen in signaling and metabolism (Gutiérrez et al., 2007; Nunes-Nesi et al., 2010), it is likely that RSA responses to mineral soil nutrients are also integrated with the plant carbon status and hence depend on light intensity and daylength. Clearly, without a quantitative phenotypic assessment of roots subjected to multiple combinations of nutritional factors, we cannot even start to understand the complex interaction between environment and development.

In this study, we quantified 13 RSA parameters in 32 conditions resulting from all binary combinations of nitrate (N), phosphate (P), potassium (K), and sulfate (S) supply and two light regimes. The concentrations tested for each nutrient were selected on the basis of a literature survey to represent sufficiency (but not inhibitory oversupply) and starvation (but not lethal deficiency). Moderate starvation was applied here to favor adaptive responses over deficiency symptoms. The chosen concentrations therefore represent physiologically relevant low- and high-affinity ranges of the primary uptake systems. Complemented with root transcriptomics and shoot ionomics, the obtained data set generates a quantitative framework describing the relationship between the multifactorial inputs and outputs. As a proof of principle, two RSA responses were selected for mutant analysis, leading to the identification of signaling modules linking K and nitrate supply with specific RSA features.

RESULTS

Root Architecture Parameters Show Distinct Patterns of Nutrient Dependence

A total of 508 *Arabidopsis* seedlings (at least 10 per condition) were grown on vertical agar plates and subjected to 32 conditions, consisting of 16 combinations of N (nitrogen in the form of nitrate only), P, K, and S supply and two light regimes (as a proxy for carbon [C]). Individual macronutrients in the media were either in sufficient (2 mM N, 0.5 mM P, 2 mM K, and 0.25 mM S) or low (0.05 mM N, 0.02 mM P, 0.05 mM K, and 0.025 mM S) supply with combinations ranging from fully sufficient (NPKS) to fully starved (npks) and including single, double, and triple starvation (e.g., NpKs; Supplemental Table 1). Light was supplied at moderate intensity for 16 h (long day [LD]) or for 9 h (short day [SD]). Plates were scanned 10 d after germination (DAG) and the 13 RSA parameters listed in Table 1 (and shown in Supplemental Figure 1) were measured using EZ-Rhizo software (Armengaud et al., 2009b). All raw data are provided in Supplemental Data Set 1. This phenotypic data set was subjected to different types of statistical analyses, including analysis of correlation (Supplemental Table 2), principal component analysis (Supplemental Figure 2 and Supplemental Table 3), and ANOVA (Figures 1 and 2; Supplemental Data Set 2).

Table 1. RSA Parameters Quantified in This Study

Abbreviation	Unit	Description
TRS	cm	TRS: sum of path length of the MR and LRs
MRP	cm	MR path length
Basal	cm	Basal zone length: MR path length from root-hypocotyl junction to first LR
Branched	cm	Branched zone length: MR path length from first to last LR
Apical	cm	Apical zone length: MR path length from last LR to MR tip
MR angle	°	MR angle: angle between the MR vector and verticality
LRS	%	LR size: sum of path length of LRs as fraction of TRS
1st Order LR no.		Number of first-order LRs (emerging from the MR)
2nd Order LR no.		Number of second-order LRs (emerging from first-order LRs)
LRP 0.25	cm	Mean LR path length in basal quarter of MR (0 to 25% of the MR)
LRP 0.50	cm	Mean LR path length in second quarter of MR (25 to 50% of the MR)
LR density/MR	cm^{-1}	LR density: 1st order LR no. divided by MRP
LR density/BZ	cm^{-1}	LR density: 1st order LR no. divided by branched

See Supplemental Figure 1 for a schematic representation of the RSA parameters listed here. BZ, branched zone.

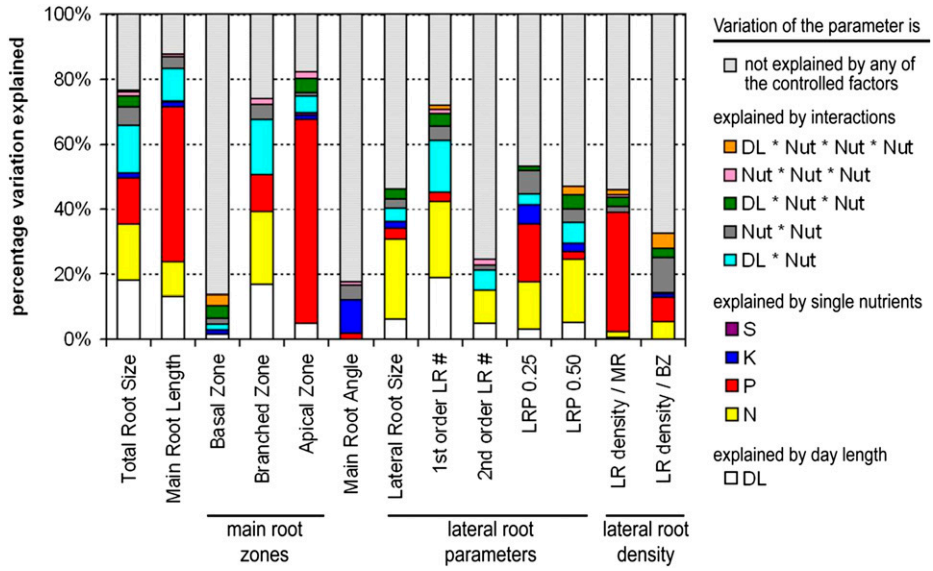

Figure 1. Variation in RSA Parameters Explained by Environmental Factors and Their Interactions.

Data shown was obtained by five-way ANOVA of RSA data from 508 plants measured 10 DAG. Individual RSA parameters (as defined in Table 1) are given on the *x* axis. Variation is given as percentage of total variation measured for an individual parameter. Environmental conditions are color-coded as shown in the legend on the right. ANOVA was computed using type-III SS at a significance level of $P < 0.05$. SS and P values are provided in Supplemental Data Set 2. DL, daylength; Nut, nutrient; *, interaction.

ANOVA was used to determine how much of the variation in each RSA parameter could be ascribed to one or more environmental variables. ANOVA is based on variance partitioning; variance of each RSA parameter, calculated as sum of deviation square (SS) from the overall mean, is split into a "between-group" component (dependent on treatment) and a "within-group" component (unexplained variation). The former is then compared with the latter using a statistical test to identify significant environmental effects. In an iterative procedure the model (here, Type III-SS) is calculated repeatedly and at each step factors with nonsignificant effects ($P > 0.05$) are eliminated until only significant effects remain. The results from the final calculation step are provided in Supplemental Data Set 2. The SS for each significant effect and for the cumulative nonsignificant effect were then related to the total sum of SS, set to 100%. We first performed a five-way ANOVA for each RSA parameter measured at 10 DAG with daylength, N, P, K, and S as the five environmental variables, each occurring at two levels (high and low). Figure 1 displays the results from this analysis plotting variation explained by environmental factors (in color) and cumulative unexplained variation (in gray) against individual RSA parameters. Predominant single nutritional factors determining the variation of RSA parameters were P and N, with a stronger influence of P on main root (MR) parameters and of N on lateral root (LR) parameters. Change of K alone had a minor effect on RSA apart from its effects on MR angle and LR path length in the basal quartile of the MR (LRP 0.25). S had no effects on RSA on its own. However, both K and S contributed to the variation of RSA parameters through interaction with other nutrients and/or daylength (see below).

Some RSA parameters were strongly determined by the environmental factors, while others were less so. For example, differences in nutrient or light explained over 70% of the variation in MR path length, apical zone length, branched zone length, and number of first-order LRs but <25% of the variation in basal zone length, MR angle, and second-order LR number. All RSA parameters depended on more than one of the varied environmental factors, and each RSA parameter showed its own typical pattern of dependence. For example, length of the apical zone of the MR was almost entirely determined by P-supply, and the MR angle was primarily determined by K. By contrast, length of LRs (e.g., in the basal quartile of the MR; LRP 0.25) was more equally influenced by P, N, and K.

Light Makes an Important Contribution to the N Sensitivity of the Root Architecture

Interactive effects of daylength and nutrient supply made an important contribution to the total RSA variation (explaining 16% of variation in branched zone length and 19% of variation in first-order LR number; Figure 1). We therefore performed four-way ANOVA (using N, P, K, and S as environmental variables) separately for the RSA data obtained from plants grown for 10 d in LDs (LD 10 DAG; 200 plants) and in SDs (SD 10 DAG; 308 plants). In order to account for different total root sizes (TRSs) of plants grown in LD and SD an additional data set recorded from SD plants after 14 d (SD 14 DAG; 289 plants) was also analyzed. The results are shown in Figure 2. TRS of SD plants doubled between 10 and 14 DAG (Figure 3), and more of the RSA variation was explained by nutrients at 14 DAG than at 10 DAG. Nevertheless, the overall nutrient-dependence pattern was

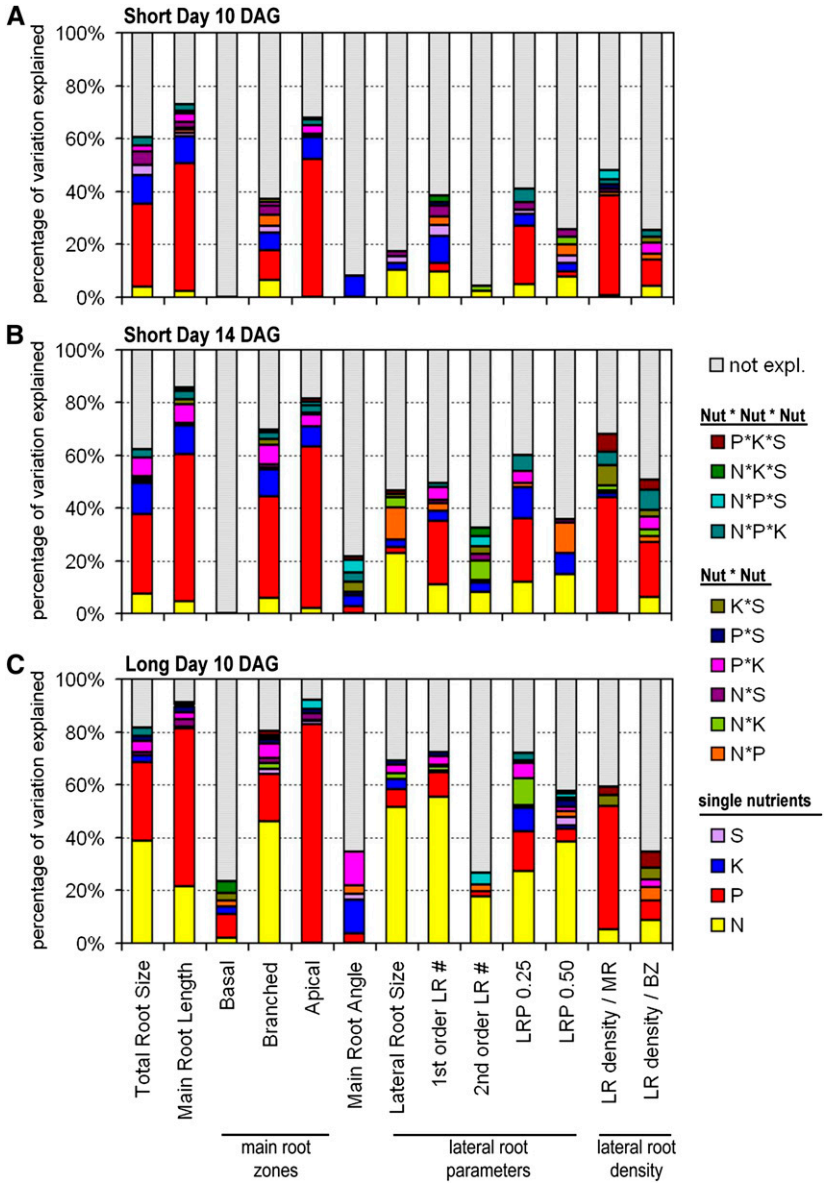

Figure 2. Variation in RSA Parameters Explained by Nutritional Factors and Their Interactions in SD and LD Conditions.

Data shown was obtained by four-way ANOVA of RSA data from plants grown in SDs for 10 d (n = 308) **(A)**, SDs for 14 d (n = 289) **(B)**, and LDs for 10 d (n = 200) **(C)**. Individual RSA parameters (as defined in Table 1) are given on the x axis. Variation is given as percentage of total variation measured for an individual parameter. Environmental conditions are color-coded as shown in the legend on the right. ANOVA was computed using type-III SS at a significance level of $P < 0.05$. SS and P values are provided in Supplemental Data Set 2. DL, daylength; Nut, nutrient; *, interaction.

similar at the two time points with P being the most important nutritional factor determining RSA in SDs both at 10 DAG and at 14 DAG (Figures 2A and 2B). TRS of LD plants at 10 DAG was similar to that of SD plants at 14 DAG (Figure 3). However, the nutrient dependence of RSA was markedly different between LD and SD plants due to an increased influence of N on RSA in LDs (Figure 2C). In particular, length and number of LRs were now primarily determined by N.

The influence of daylength on RSA was further demonstrated by additional statistical tests. Supplemental Table 2 details the results of a Pearson analysis of correlations between different RSA parameters. Correlations are maintained between LD and SD conditions showing that differences in daylength did not uncouple the general pattern of interdependency between RSA features (Supplemental Table 2). However, principal component analysis (PCA) clearly distinguished between plants grown in SD and plants grown in LD (Supplemental Figure 2). PCA identifies subsets of RSA parameters (principal components [PCs]) that significantly differentiate between the samples. Plotting the individual samples (nutrient treatments) against the PCs provides

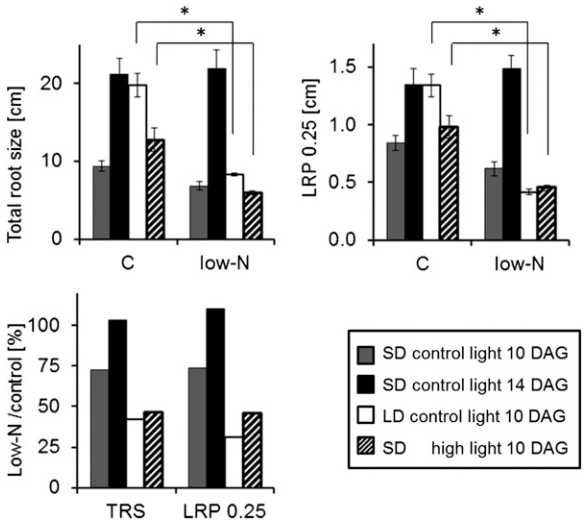

Figure 3. High-Light Intensity over SDs Elicits Similar Root Responses to Nitrate Starvation as Moderate Light Intensity over LDs.

TRS and LR path length in the first basal quartile of the MR (LRP 0.25) in control and low-N media. Plants were grown in three light regimes: SD with control (moderate) light intensity (160 μmol m^{-2} s^{-1}; gray and black bars), LD with control light intensity (white bars), and SD with high-light intensity (280 μmol m^{-2} s^{-1}; dashed bars). RSA parameters were measured 10 or 14 DAG as indicated. The total light dose was the same in SD 14 DAG control light, LD 10 DAG control light, and SD 10 DAG high light. Bars show means (n = 11 to 22 plants) ± SE. Different letters indicate significant differences at $P < 0.05$ (Tukey's t test). Ratios of the means (control/low-N) are shown in the bottom graph.

a measure of how similar/different root architectures were between the treatments. For SD plants, PC1 and PC2 (explaining together 80% of the variation in the samples) positioned low-K and low-P treatments (alone and in combinations with low-N and low-S) well away from the control, whereas low-N (alone and in combination with low-S) clustered with the control. By contrast, for LD plants, low-N treatments (alone and in combination) were well separated from the control particularly by PC2. Supplemental Table 3 lists the contributions of individual RSA parameters to the PCs, showing that PC1 was predominantly composed of MR parameters, while PC2 was predominantly composed of LR parameters. Apart from confirming the dependence of N-effects on daylength, the PCA also confirmed that comprehensive quantification of RSA has diagnostic value for distinguishing between nutrient conditions in the root environment.

To investigate whether RSA differences between SD and LD plants were caused by differences in diurnal rhythm or photon input, we grew plants in SDs with a higher photon flux density of 280 μmol m^{-2} s^{-1} (high light) compared with 160 μmol m^{-2} s^{-1} given to control plants (control light). Over 10 d, the high light in SD produced the same cumulative photon dosage as the control light in LD. The results shown in Figure 3 indicate that high photon dosage was indeed the primary factor determining N-dependence of RSA. While roots grown with high light over SDs did not reach the same total size as roots grown in control light over LDs, they mimicked the latter by showing a strong response to N-starvation (>50% reduction in TRS and LRP 0.25). We conclude that light enhances the sensitivity of RSA to N-starvation.

Combinatorial Effects of Nutrients and Daylength on RSA Reveal a Complex Network of Crosstalk

ANOVA revealed statistically significant interdependent influences of two or more nutrients on RSA (Figures 1 and 2). Effects of double versus single deficiencies can be visualized and compared by plotting the relative response of every RSA parameter in a radar chart where each RSA parameter is represented by the spoke of a wheel. The size of each parameter in control conditions is set to 100%, and the changes of root architecture induced by the treatments are reflected in distortions from the 100% circle. Figure 4 shows a radar chart for RSA responses to low-N in SDs, overlaid with those for low-P and low-NP (Figure 4A), low-K and low-NK (Figure 4B), or low-S and low-NS (Figure 4C). The overlays show that the double deficiencies produced root architectures that were not solely explained by independent additive effects of the individual deficiencies. Depending on the individual RSA parameter, double starvation could prioritize or potentiate the effect of single deficiencies or even produce opposite effects to those produced by the single deficiencies. For example, compared with single N- or P-starvation, double NP-starvation had a potentiating effect on apical length inhibition and on LRP 0.25 and an opposite (inhibitory versus stimulating) effect on LRP 0.5 (Figure 4A). Double NK-starvation potentiated several inhibitory effects of K-starvation, although the respective RSA parameters (length of branched zone, LRP 0.5, and TRS) were not affected or even increased by N-starvation (Figure 4B). A strong stimulating effect of low-K on second-order LRs did not occur in low-NK (Figure 4B). An increase of LRP 0.5 in low-N was absent in low-NS, although low-S alone had no effect on this parameter (Figure 4C). Double NS starvation increased the number of second-order LRs, although each individual starvation slightly reduced this parameter. A detailed description of all nutrient interactions in this text is not possible, but interested readers can explore radar charts for any conditions of their choice using the Excel file and manual provided as Supplemental Data Set 3.

The ANOVA analysis also highlighted higher-order interactions between several nutrients and daylength; however, it did not reveal the exact nature of these interactions (e.g., stimulating and inhibitory). A more detailed analysis of interdependent effects was performed for two well-defined RSA parameters that strongly determine TRS: LR path length in the basal quartile of the roots (LRP 0.25) and length of the apical zone of the MR (Figure 5). The average lengths of LRP 0.25 and apical zone across all conditions are shown in Figures 5A and 5B, and P values for all pairwise comparisons are listed in Supplemental Tables 4 and 5. Based on these data, the nature of interactive effects between the various environmental inputs on the measured phenotype can be described in logical terms (Figure 5C). For example, low N inhibits LRP 0.25 but only if one of the following conditions is present as well: LDs, low K, or low P. Low K or low P also inhibit LRP 0.25 in sufficient N but in this case require either low S or LDs to occur as well. Low P inhibits apical zone length on its own, but low N, low K, low S, and LDs all

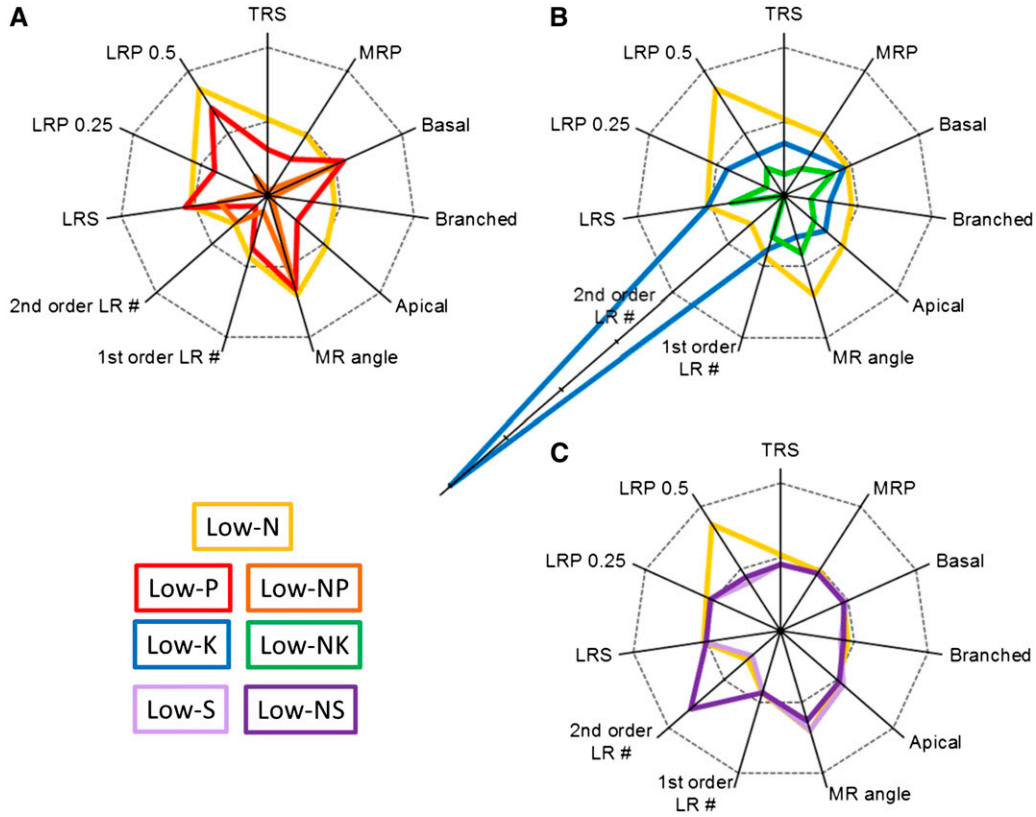

Figure 4. Effects of Single and Double Nutrient Starvation on RSA.

The effects of individual and double nutrient starvation on RSA, visualized as radar charts. Low-N (yellow), low-P (red), and low-NP (orange) **(A)**; low-N (yellow), low-K (blue), and low-NK (green) **(B)**; low-N (yellow), low-S (light purple), and low-NS (dark purple) **(C)**. RSA data are from plants grown in SDs for 14 DAG. The mean of each RSA parameter in a given medium was normalized to the mean of the same parameter measured in the control medium (sufficient NPKS). The dashed lines indicate a ratio of 1 (inner line = control) or 2 (outer line). Abbreviations of RSA parameters are as in Table 1. Raw data and radar graphs for other nutrient combinations are available in Supplemental Data Set 3.

enhance this effect. Apical zone length is also inhibited if either K alone or both N and K are low but both of the effects are only visible in SDs. Finally, a triple combination of low N, low S, and LDs also inhibits apical zone length. Even the simple scheme depicted here illustrates the complexity of interdependences between nutrient starvation response pathways. Our results provide a set of defined conditions and phenotypes that can now be used to identify the molecular components underlying nutrient signaling crosstalk through the analysis of mutants or natural genetic variation.

It is important to note that not all RSA parameters were responsive to changes in the environment. Thus, LR density over the branched zone was very similar in all conditions, and it was particularly insensitive to changes of daylength (Figure 6). The robustness of this feature stresses its suitability for root developmental studies.

Two Distinct K/N Signaling Modules Regulate LR Branching and MR Angle

To assess whether the obtained data can be used to identify novel signaling modules, we performed additional RSA phenotyping of mutants defective for genes with known roles in K and nitrate transport/ signaling. N-K interactions are important in the field and are apparent in primary metabolism (Armengaud et al., 2009a). However, the molecular players of K-N signaling crosstalk have not yet been clarified genetically. Analysis of RSA in control and low-K conditions revealed significant K-dependent mutant effects on second-order LR number and MR angle (Supplemental Figures 3A and 3B). Figure 7A shows second-order LR number normalized to the average length of first-order LRs (to account for any differences in first-order LR length between genotypes or media). Second-order LR formation was significantly stimulated by K-starvation in wild-type plants (Columbia-0 [Col-0]), and a similar response was measured in *hak5* and *nrt2.1* mutant plants, which are defective in the main high-affinity transporters of K and nitrate, respectively. By contrast, induction of second-order LRs by low-K was significantly weaker in mutant plants defective for the K-channel AKT1 (*akt1*). This finding is surprising since AKT1 is not required for K-nutrition in low-K as long as HAK5 is functional (Rubio et al., 2008). Nevertheless, a role of AKT1 was further supported by the observation that induction of second-order LRs by low-K was completely abolished in mutant plants defective for the

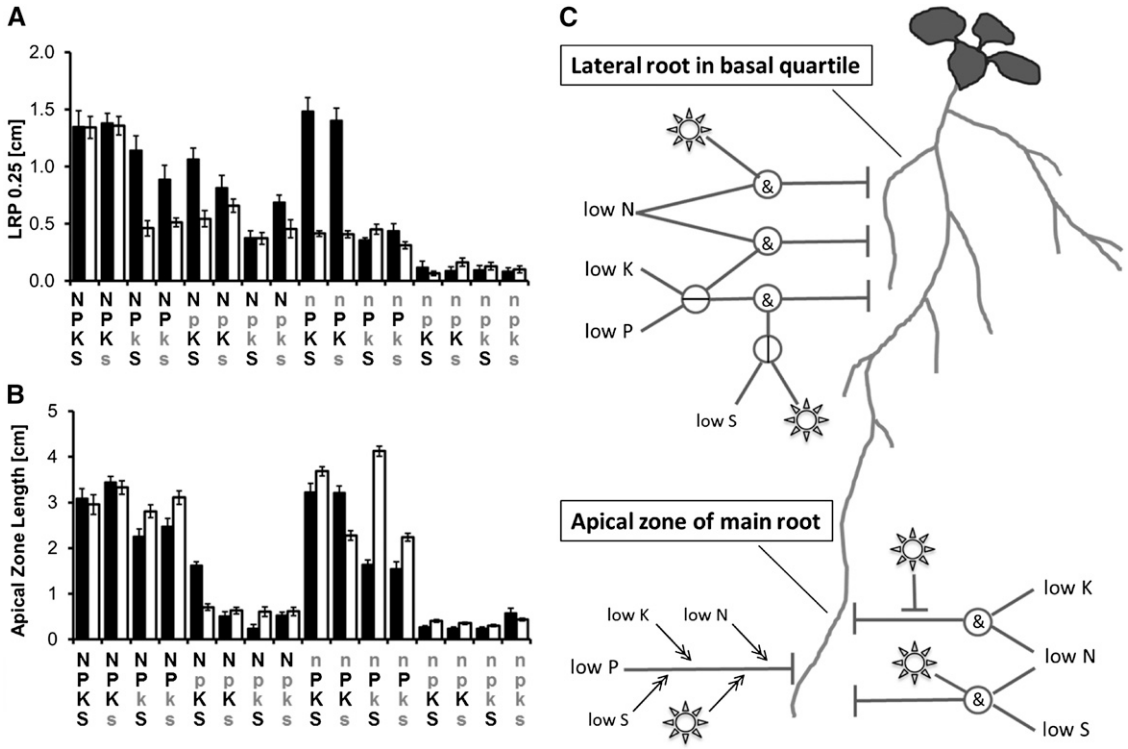

Figure 5. Interactive Effects of Nutrients and Daylength on Lateral and MR Path Length.

Average length of first-order LRs **(A)** in the basal quartile of the MR (LRP 0.25) and of apical zone of the MR **(B)** across different nutrient conditions in SDs (filled bars; 14 DAG) or LDs (open bars; 10 DAG). The 16 nutrient combinations in the media are indicated with uppercase letters for nutrients in sufficient supply and lowercase letters for nutrients in low supply. Bars are means ± SE of at least 10 plants per condition. Interdependent effects of nutrients and daylength are summarized in **(C)** using the following formalism: T-bars for inhibition, double arrows for enhancement, circled & for logical AND gate, circled line for logical OR gate. LD condition is represented with a sun. All depicted relationships are based on significant differences of the average values at $P < 0.05$. P values for all 16 × 16 pairwise comparisons obtained with Tukey's *t* test are shown in Supplemental Tables 4 and 5.

CBL-interacting protein kinase CIPK23, which is known to activate AKT1 (Li et al., 2006; Xu et al., 2006). A small reduction in the response of LR branching to low-K was also recorded in *chl1-5* mutants defective in the nitrate transporter/receptor NRT1.1, another known target of CIPK23 (Ho et al., 2009). This was again unexpected because low-N inhibited induction of second-order LR formation by low-K (Figure 5B). However, decreasing the concentration of nitrate in a constant background of sufficient nitrogen (through replacement with Gln or ammonium) induced second-order LR formation (Supplemental Figure 3C). The nitrate-specific induction occurred over a concentration range that triggers phosphorylation of NRT1.1 by CIPK23 (Ho et al., 2009). The results identify second-order LR formation as a phenotypic readout for crosstalk between K and nitrate signaling. CIPK23 emerges as connective node acting through both AKT1 and NRT1.1 (Figure 7B), a function that had been proposed (Tsay et al., 2011) but so far lacked experimental evidence. Since AKT1 and NRT1.1 are not essential for K or nitrate nutrition in the given conditions, both proteins seem to function primarily as nutrient sensors in this response.

Growth of *Arabidopsis* Col-0 roots on a two-dimensional agar surface leads to a consistent deviation of the MR axis, which is toward the right when monitored from the back of the plate through the agar. The exact molecular basis of the skewing phenomenon is not known, but several explanations have been proposed (see Discussion). Figure 7C shows MR angles in wild-type and mutant plants. A positive sign was given to roots slanting to the right, which was the case for wild-type plants as well as *hak5*, *cipk23*, and *chl1-5* plants in control (K-sufficient) conditions. Significantly different angles in control conditions were displayed by *akt1* plants, which showed a mean negative MR angle, and by *nrt2.1* plants, which displayed a more positive MR angle than wild-type plants (Figure 7C). In low-K, the mean MR angle changed from positive to negative values in all genotypes. The combined evidence identifies an essential role of (sufficient) K in imposing a positive growth angle on the MR and an essential role for AKT1 in mediating this effect. Lack of K or lack of AKT1 drives the angle to the left. The fact that control *akt1* plants did not phenocopy low-K wild-type plants for other RSA features (Figure 7D; Supplemental Figures 3A and 3B) indicates that the MR angle phenotype of *akt1* in control media is not due to impaired K-nutrition. Indeed, additional transport systems contribute to low-affinity K-uptake in high K (Rubio et al., 2010). The role of AKT1 in determining MR angle is therefore again related

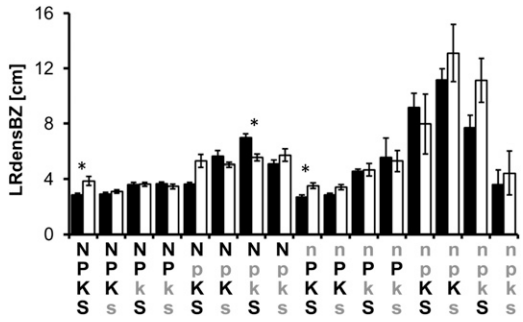

Figure 6. LR Density in Different Nutrient and Light Conditions.

LR density within the branched zone (LRdensBZ) of plants grown in SDs (filled bars; SD 14 DAG) or LDs (open bars; LD 10 DAG). Composition of the 16 nutrient combinations in the media is indicated with uppercase letters for nutrients in sufficient supply and lowercase letters for nutrients in low supply. Bars are means ± SE of at least 10 plants per condition. Significant differences between SD and LD plants in the same media are indicated with asterisks ($P < 0.05$; Tukey's *t* test).

to sensing/signaling rather than K-nutrition. However, unlike in the case of LR-branching, this function of AKT1 is independent of its phosphorylation by CIPK23, and it does not involve NRT1.1. Interaction between nitrate and K is nevertheless apparent in the fact that lack of NRT2.1 drives the angle to the right. Thus, NRT2.1 has an opposite effect to AKT1, and the net MR angle in control conditions is the result of both effects (Figure 7E). Low-K overrides this balance, leading to a negative angle independent of whether NRT2.1 is functional or not. In summary, we found that two distinct RSA features are regulated by different subsets of the K/nitrate signaling network.

Coregulated Gene Clusters Match Nutrient Response Signatures

To extend the pool of candidate components of the nutrient signaling network, we determined genome-wide transcriptional changes in response to multiple combinations of nutrient deficiencies. Eight different media composed of all combinations of sufficient/deficient N, P, and K were used. S was sufficient in all media (as it had only minor effects on RSA), and all plants were grown in LDs (to enhance N-effects). To capture early responsive genes that may initiate differential root development, plants were harvested after 6 d of growth. RNA was extracted from root tissue from three independently grown batches of seedlings (biological replicates) and hybridized to microarrays. Normalized signal intensities measured in each condition and mean transcriptional responses for each gene are provided as Supplemental Data Set 4. After discarding genes with overall low mRNA levels, 371 genes showed a significant change of at least 4-fold in at least one nutritional condition. Hierarchical clustering of these nutrient-responsive genes based on their response profiles across the conditions showed a clear separation between genes that were generally upregulated (142 genes) and genes that were generally downregulated (228 genes) by nutrient starvation (Supplemental Figure 4).

Clusters of coregulated genes were identified by k-means analysis of transcript changes across the nutrient conditions. To allow for subsequent comparison with RSA profiles, magnitude independent Pearson correlation was used. Assignment of nutrient selective genes into 38 clusters (19 UP and 19 DOWN clusters; Supplemental Figures 5 and 6) efficiently separated different response profiles without generating too many similar clusters. Representative examples are shown in Figure 8. Each gene had its own specific profile, but a few general trends can be highlighted as distinctive features of the clusters: (1) increasingly strong response to low-K, low-P, and low-N with additive effects of each nutrient deficiency (34 genes in UP1 and 37 genes in DOWN1, also 18 genes in UP2 and UP3, 15 genes in DOWN2 and DOWN3); (2) strong response to low-N with weak individual or added effects of low-K or low-P (27 genes in UP4 and 40 genes in DOWN4, also 13 genes in UP5 and UP6); (3) strong response to low-N with strong additive effect of low-K (37 genes in DOWN7, also 54 genes in DOWN8 and 1 gene in DOWN9); (4) weak response to individual nutrient deficiencies but strong response to dual or triple deficiencies (11 genes in UP7); (5) strong response to low-P and low-N with additive effects (17 genes in DOWN10, 17 genes in UP10, also five genes in UP8); (6) strong response to low-P with or without additive effects of low-N or low-K (seven genes in UP13, one gene in DOWN13, also nine genes in UP11, UP12, UP14, and UP15 and two genes in DOWN 12); (7) strong response to low-K, similar or weaker response to low-P and low-N (one gene in UP16 and one gene in DOWN16); (8) selective response to low-K (one gene in UP19), low-N (two genes in DOWN6), or low-K and low-N (one gene in DOWN 18 and two genes in DOWN19). Genes assigned into the clusters are listed in Supplemental Data Set 5. The gene clusters contained individual subsets of genes related to primary C-N and P metabolism, cell wall synthesis and expansion, as well as water and nutrient transport, likely to represent the growth responses triggered by each nutrient deficiency. Furthermore, many regulatory genes such as transcription factors and kinases were found, particularly among upregulated genes, as well as many genes with hitherto unknown function.

An obvious question was whether the obtained transcriptional profiles matched response profiles of individual RSA features. To approach this question, we selected mean RSA responses for the subset of conditions used in the microarray analysis and calculated Pearson correlation to the mean response profiles of the identified transcript clusters. As shown in Table 2, the analysis revealed several significant correlations. For example, the nutrient response profiles of MRP and other MR-related parameters correlated with those of UP7, UP10, and DOWN14 clusters, characterized by similar responsiveness to low-N and low-P and strong response to double and triple deficiency. By contrast, LRS and LRP 0.5 profiles best matched those of UP4 and DOWN4, which were dominated by a strong response to low-N with little additive effects of low-K or low-P. The length of the apical zone correlated with UP8, UP15, DOWN12, and DOWN14, which showed a particularly strong response to low-PK double deficiency. The identified gene clusters therefore provide a useful pool of candidate genes that underpin the responses of individual RSA features to different combinations of N, P, and K.

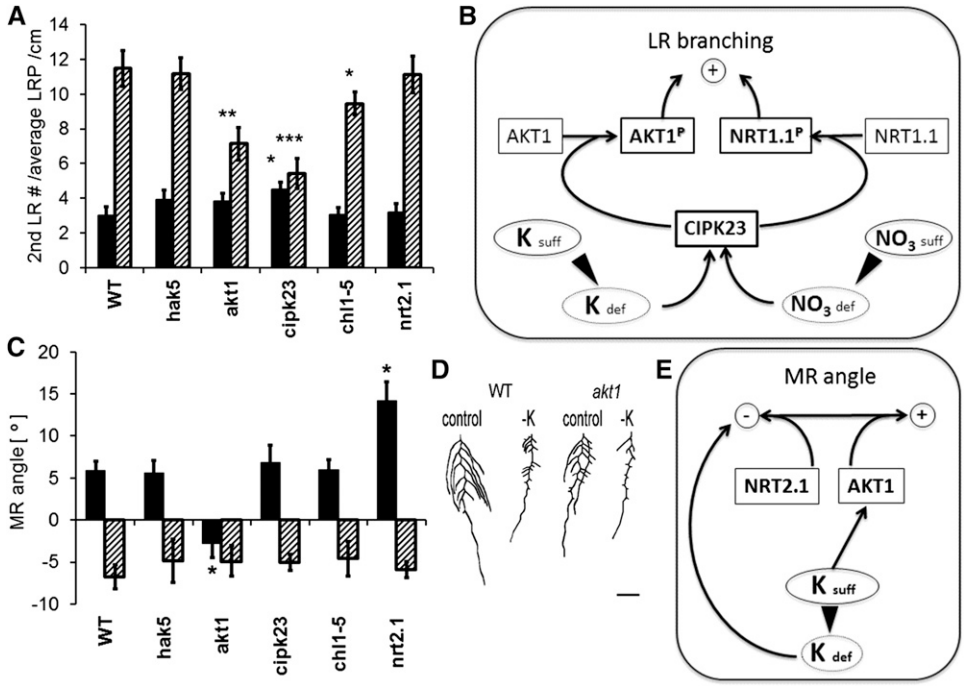

Figure 7. K and Nitrate Signaling Components Collaborate in the Regulation of LR Branching and MR Angle.

(A) Number of second-order LRs normalized to the mean LR path length of wild-type and mutant plants grown on control (black bars) and low-K (dashed bars) media in SDs. Bars are means ± SE of at least 20 plants per genotype and condition. Significant difference from the wild type in the same condition is indicated with asterisks: *P < 0.05; **P < 0.01; ***P < 0.001.

(B) Proposed model: A change of K or nitrate from sufficient (suff) to deficient (def) supply activates CIPK23 (possibly via a rise in cytoplasmic Ca), which in turn phosphorylates AKT1 and NRT1.1 to AKT^P and $NRT1.1^P$, both of which stimulate second-order LR emergence.

(C) MR angle of wild-type and mutant plants grown on control (black bars) and low-K (dashed bars) media. Bars are means ± SE of at least 13 plants per genotype and condition. Significant difference from the wild type in the same condition is indicated with asterisk: *P < 0.001.

(D) Representative images of root phenotypes of wild-type and *akt1* plants in control and low-K. Bar = 1 cm.

(E) Proposed model: AKT1 and NRT2.1 drive the MR angle to the right and left, respectively, thereby determining the net angle in control conditions. Knockout of NRT2.1 shifts the balance toward AKT1 (right angle), and knockout of AKT1 shifts the balance toward NRT2.1 (left angle). Low-K also drives the angle to the left, but this response is not reverted by knockout of NRT2.1.

Single and Multiple Deficiencies Alter Shoot Ionome Profiles

RSA responses will ultimately determine the nutritional status of the shoots and vice versa. A comprehensive study into the reciprocal relationship between RSA features and shoot nutrient status requires measurement of RSA, shoot weights, and ion concentrations in the same individual plants, which was not possible in this noninvasive study. However, to allow future integration of shoot data with our data set, we measured shoot ion concentrations from pooled plant samples grown in the same subset of conditions that were used for the microarray experiments (NPK combinations, LD, and 10 DAG). Three replicate batches of independently grown plants were analyzed by inductively coupled plasma mass spectrometry (ICP-MS) for each condition. Results are shown in Figure 9 and Supplemental Figure 7. As expected, P starvation reduced shoot P concentration ([P]), and K-starvation reduced shoot [K]. Other ions showed parallel or antiparallel changes, most likely to reflect an adjustment of ionic charges. Thus, low-P (phosphate) and low-N (nitrate) decreased shoot concentrations of K, Ca, Mg, and Na. By contrast, low-K strongly increased shoot concentrations of Ca, Mg, and Na. In accordance with a charge balancing role, shoot accumulation of these cations in low-K was less pronounced if N and P were also low. Concentrations of cationic micronutrients were generally lower in low-P and low-N, whereas low-K produced slightly increased concentrations of Mn and Zn (Supplemental Figure 7). The most conspicuous change was a dramatic increase of the shoot Fe concentration in low-P and low-N, which was further enhanced by NP-double starvation (15- to 20-fold; Figure 9). Furthermore, the shoot Fe concentration across the eight conditions showed a significant negative Pearson correlation with the total size of the root system (TRS) and the length of the branched root zone ($P < 0.01$), indicating that the plant Fe status might have an effect on RSA. None of the other shoot ion concentrations showed a correlation to any of the RSA parameters and neither did the shoot fresh weight (data for shoot fresh weight is shown in Supplemental Figure 7). However, when shoot ion concentrations were related to shoot

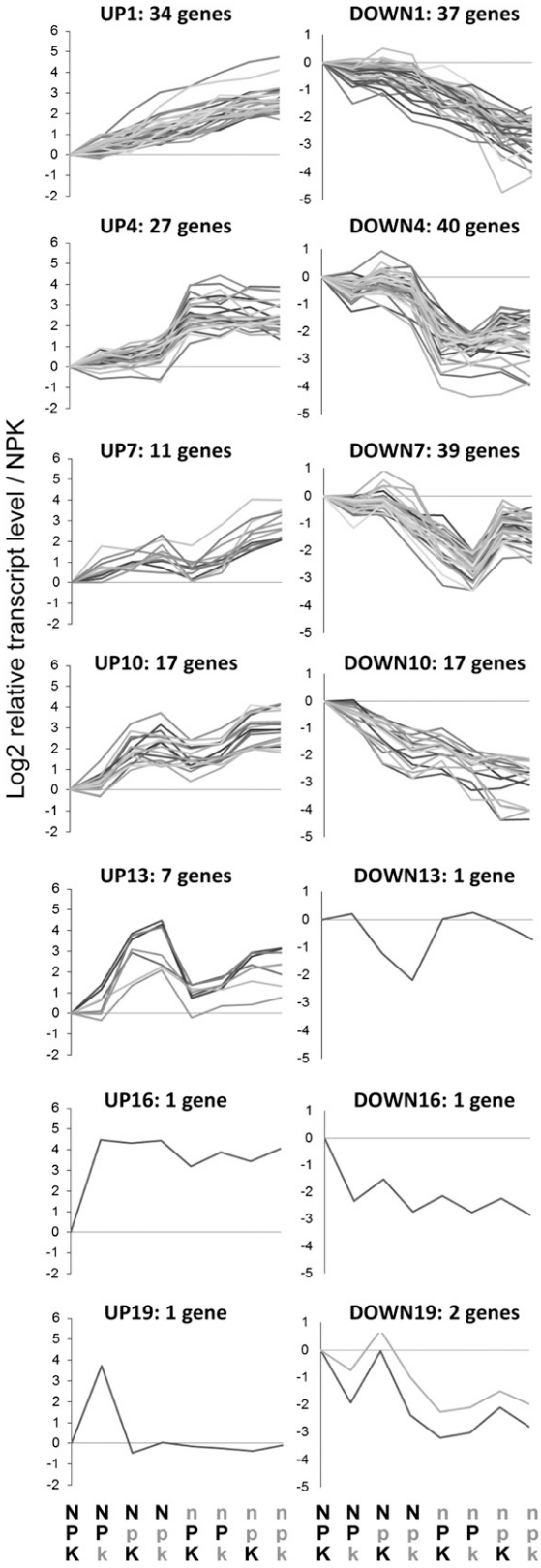

Figure 8. Expression Profiles of Root Genes in Selected UP and DOWN Clusters in Response to Different Combinations of N, P, and K Supply.

Data shown were obtained by microarray analysis of RNA from root tissue sampled 6 DAG in eight conditions of sufficient (uppercase) or low (lowercase) NPK supply as detailed at the bottom of the figure. For each condition, mean transcript levels in three biological replicate samples were determined after signal normalization across arrays. Based on several criteria (false discovery rate < 0.01, transcript signal > 100, fold change (treatment/control) > 4 in at least one condition), 371 nutrient-responsive genes were identified, separated into up- and downregulated genes (Supplemental Figure 4), and subjected to k-means clustering by Pearson correlations. Each graph shows the mean transcriptional response profiles of the genes in a particular cluster. Responses are expressed as $\log_2$ of the ratio of transcript levels in a given nutrient condition versus control (NPK). All 38 clusters are shown in Supplemental Figures 5 and 6. Gene identifiers, transcript ratios, and standard errors for all clusters are provided in Supplemental Data Set 5.

fresh weight, absolute ion shoot contents of P, Ca, Mg, Na, Mn, and K were found to positively correlate with the number of LRs ($P < 0.05$), suggesting that the number of LRs might determine the overall uptake of these ions into the plant.

DISCUSSION

Multifactorial Nutritional Experiments Generate Important Information

Availability of mineral nutrients in the soil is one of the main factors limiting high-intensity crop production, which therefore heavily relies on fertilization. The importance of plant mineral nutrition for human food production is reflected in a long history of research in this area. To date, we have a detailed understanding of the transport, signaling, and metabolic pathways that allow plants to adapt to fluctuating nutrient availability in the soil (Amtmann and Blatt, 2009; Armengaud et al., 2009a; Giehl et al., 2009; Gojon et al., 2009). However, until now, effects of individual nutrients have mostly been studied in isolation. This experimental approach does not reflect the field situation in which deficiencies of several nutrients occur simultaneously and in various combinations. The question of how signaling pathways for several individual nutrients interact has not been studied systematically. We have shown here that nutrient interactions can be quantified through a multifactorial experimental design and that root system architectural responses provide an excellent phenotypic readout for these interactions. A binary approach offering each macronutrient (N, P, K, and S) in one sufficient and one low concentration in either short or long days (as a proxy for C) can only be the beginning of such research. RSA responses are not necessarily linear over a wider range of concentrations (Gruber et al., 2013), and macronutrients signals will not only be integrated with each other but also with information on micronutrient availability and other environmental factors. Furthermore, the time course of nutrient depletion both outside and inside the root will differ for individual nutrients depending on uptake kinetics, root-shoot allocation, and availability of internal stores. More time points should therefore be analyzed in the future. Nevertheless, the results

Table 2. Correlations between Mean Response Profiles of Gene Clusters and RSA Parameters

	UP 1	UP 4	UP 7	UP 8	UP 10	UP 14	UP 15	
TRS[a]			−0.96		−0.87			
MRP			−0.94		−0.88			
Branched			−0.95		−0.88			
Apical				−0.87			−0.84	
LRS		−0.88						
LRP 0.25			−0.88					
LRP 0.5		−0.91						
1st Order LR no.	−0.90		−0.89					
LR density/MR						0.91	0.89	
LR density/BZ			0.97	0.89	0.88			
	DOWN 1	DOWN 4	DOWN 5	DOWN 8	DOWN 10	DOWN 12	DOWN 14	DOWN 17
TRS	0.86							
MRP							0.96	
Branched	0.91				0.85		0.88	
Apical						0.91	0.90	
LRS		0.90						
LRP 0.25			0.85				0.89	
LRP 0.5		0.96		0.89				
1st Order LR no.	0.95		0.93		0.88			
LR density/MR								
LR density/BZ						−0.88		−0.83

Numbers given are Pearson correlation coefficients. Only significant correlations at $P < 0.01$ are shown. BZ, branched zone.
[a]For definitions of RSA parameters, see Table 1.

presented already provide an ample resource for the study of integrative nutrient sensing and signaling.

Fundamental findings from the presented multifactorial data set can be summarized as follows. (1) We have shown that each RSA feature shows a typical pattern of sensitivity to individual and combined nutrient starvation, thereby identifying the critical RSA parameters that represent the phenotypic output for different parts of the underlying signaling network. (2) The specific conditions under which interactive effects occur have been identified thereby guiding the experimental design of future analyses of molecular crosstalk. (3) We discovered nutrient sensitivity of RSA features such as LR length in different parts of the root system and MR angle, thereby providing additional opportunities for studying the pathways that mediate between nutrient signals and specific developmental processes. (4) Transcriptional responses across eight combinations of N, P, and K supply fell into distinct response profiles, some of which matched those of specific RSA features. These gene clusters and their phenotypic output provide a resource for identifying the molecular entities that generate certain RSA features and the regulatory hubs that link nutrient signaling pathways. (5) Parallel analysis of total shoot ion contents in multiple nutrient combinations provides a benchmark for future studies linking specific root architectures to nutrient contents of the aboveground tissues.

RSA Parameters Differ in Their Sensitivity to Nutritional Cues

Depending on the RSA parameter measured, more or less of its variation could be explained by the environmental factors (Figures 1 and 2). In some cases, an apparently low environmental influence can be explained with technical difficulties to precisely determine the parameter, e.g., length of basal zone depends on precise determination of the root-hypocotyl border, and lengths of LRs close to the root tip (LRP 0.75 and LRP 1.00) were close to the detection limit. These parameters were not further characterized here. Another possible reason for environment-independent variation lies in the stochastic nature of the trait itself. Examples for the latter are MR angle and second-order LR number, as those parameters could be quantified with higher precision. Finally, certain RSA parameters may be regulated by developmental programs that are robust against environmental fluctuations. Thus, LR density within the branched zone was highlighted as a very stable parameter across all conditions. In particular, LR density was independent of daylength when normalized to the length of the branched zone (Figure 6). We therefore propose to make use of this parameter when studying fundamental properties of LR development as previously discussed (De Smet et al., 2012; Dubrovsky and Forde, 2012).

Commonly measured root traits such as MR length, TRS, and LR number were strongly associated with nutrient supply, but additional parameters measured here refined this output. For example, apical zone length emerged as a more precise reporter of P supply than MR length (Figures 1 and 2), and should therefore be used in genetic screens for P-response elements.

P Is the Main Factor Determining MR Growth

P starvation has been reported to elicit a dual response: a decrease in MR growth and an increase of LR growth, especially in

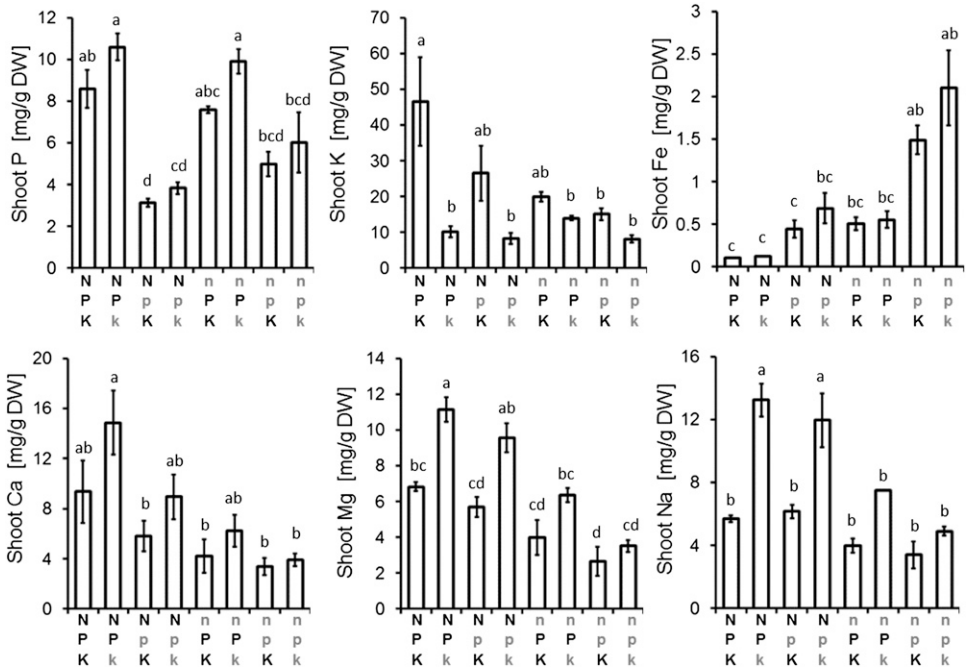

Figure 9. Shoot Ion Concentrations of Plants Grown in Different Combinations of N, P, and K.

Bar charts show shoot concentrations of P, K, Fe, Ca, Mg, and Na as quantified by ICP-MS. Shoot tissue was harvested from wild-type Col-0 plants grown in LD conditions for 10 DAG. As indicated on the *x* axes, the media contained N, P, and K in different combinations of sufficient (uppercase) and low (lowercase) supply. For each of three replicate experiments, shoots of 30 to 100 plants were pooled and dried and ions extracted by in vitro digestion. Ion concentrations were normalized to dry weight (DW). All values are means ± SE. ANOVA was computed followed by pairwise comparison corrected for multiple testing (Bonferroni's *t* test). Different letters above the bars indicate significant differences at $P < 0.05$.

the upper parts of the root system (Williamson et al., 2001; López-Bucio et al., 2002). Our results confirmed a strong inhibitory effect of low-P on MR elongation, but we did not observe LR elongation in the basal part of the root; instead, LRP 0.25 was lower in P-deficient than in P-sufficient conditions. A possible explanation is the timing of LR initiation, which happens early on in P-starvation (Al-Ghazi et al., 2003; Pérez-Torres et al., 2008) and may therefore be no longer apparent at the time points analyzed here. Indeed, one study reported a transient increase of LR initiation and elongation in low-P, followed by an overall decrease of these traits compared with control conditions (Nacry et al., 2005).

ANOVA of the entire data set showed that P was by far the most important factor regulating MR elongation independently of other nutrients or daylength (Figures 1 and 2). This argues for a prioritization of low-P responses over other mineral nutrient responses in multiple deficiencies as far as MR growth is concerned. It has been proposed that P-starvation symptoms are indirect effects of iron (Fe) toxicity due to formation of Fe-P precipitates and hence increased Fe-availability in the media (Ward et al., 2008). As reported previously (Hirsch et al., 2006), the shoot Fe concentration increased in low-P. Furthermore, across eight conditions of varying NPK supply, shoot Fe correlated negatively with TRS and length of the branched zone. Whether accumulated Fe has itself an inhibitory effect on root growth or whether it merely reflects the history of an inhibitory effect of external Fe on the root meristem of young seedlings needs now to be investigated (Ward et al., 2008).

N-Starvation Responses Depend on High Photon Input

The C/N ratio in the medium has been identified as a crucial factor for root growth (Malamy and Ryan, 2001). The strong dependence of low-N responsiveness on light observed in our study was therefore surprising since all growth media were complemented with 0.5% Suc. The calculated N/C ratio in the low-N media was 1/3509 compared with 1/88 in the control, but this decrease of the external N/C ratio did not elicit N-starvation symptoms in SDs. One possible explanation is that the carbon signal has to be shoot-derived, which was supported by the observation that high-light dosage over SDs mimicked N-dependence of RSA in LDs (Figure 3). An alternative explanation is a root-delimited pathway in which root-autonomous light sensing is coupled with N-signaling. Our growth system only allowed light from the top to penetrate through the plates to the roots and hence simulated the light gradient in a light-permeable soil. With all major photosensors present in roots, there is good evidence for root-delimited light responses (Kutschera and Briggs, 2012). Future research into the causes of light-dependent RSA responses can now build on the specific nutrient conditions and phenotypic RSA outputs identified here as being light-dependent (Figure 5). In addition, microarray analysis of roots

grown in LDs identified potential molecular players of C/N signaling in the roots. For example, the phloem-loading Suc transporter gene *SWEET12* (Chen et al., 2012) showed more than 2-fold upregulation by low-N and more than 4-fold upregulation by low-NP. Low-N also caused a more than 4-fold induction of the nitrate transporter *NRT1.8*, which recovers nitrate from the xylem (Li et al., 2010). The two transport processes work in opposite directions, reducing Suc and increasing nitrate concentrations in the root cortex. This regulation might reflect a strategy by the plant to reduce the inhibitory effects of a high C/N ratio on LR growth.

Nutrient Interactions Provide Readouts of Signaling Crosstalk

Analysis of the entire data set via ANOVA revealed significant contributions of nutrient–nutrient interactions in regulating various root architectural parameters (Figures 1 and 2). We detected two-level interactions, such as N-K, N-P, P-K, and N-S, as well as higher-order interactions of three nutrients, indicating multiple sites of crosstalk in the underlying signaling networks (Figure 6). S effects on RSA only appeared in the context of interactions. The weak effect of low-S in sufficient NPK was not due to insufficient starvation as the plants showed a significant decrease of the shoot S concentration, an increase of the shoot molybdenum concentration typically seen in S-starved plants (compared with Alhendawi et al., 2005), and induction of the low-S marker genes SULTR1.1 (Rouached et al., 2008) and SDI1 (Howarth et al., 2009) in the roots (Supplemental Figure 8). Recent RSA phenotyping over a range of nutrient concentrations also failed to detect an effect of low-S on RSA (Gruber et al., 2013). Our findings suggest that nutrient background and light conditions contributed to low-S effects observed in other studies (Maruyama-Nakashita et al., 2004; Wu et al., 2010). Importantly, our data show that S makes an important contribution to RSA through several interactions with other nutrients and daylength. Several entry points of S into the nutrient signaling network have been identified here (Figure 6) and can now be used to identify the underlying molecular components through mutant studies.

Dependence of RSA parameters on nutrient interactions provides a powerful readout for molecular studies investigating nutrient signaling crosstalk. We tested this approach for K-N interactions using mutants for several genes with known functions in transport, sensing, and/or signaling of K and nitrate in roots. Our experiments revealed roles of the K-channel AKT1 in regulating two distinct RSA parameters (second-order LR number and MR angle) within two different signaling modules.

CIPK23 Regulates LR Branching through AKT1 and NRT1.1

CBL1, CBL9, and CBL-interacting kinase CIPK23 constitute a cellular signaling pathway that links AKT1 activity to the external K concentration presumably via cytoplasmic calcium (Li et al., 2006; Xu et al., 2006). The physiological relevance of this pathway, however, has remained a mystery because AKT1 does not make a major contribution to K-uptake in low-K conditions as long as HAK5 is active (Rubio et al., 2008). Our study not only identified LR branching as a developmental, target process of this signaling module (Figures 7A and 1B), but also linked it with the nitrate-transceptor NRT1.1, another target of CIPK23 (Ho et al., 2009).

NRT1.1 has previously been implicated in the root colonization of nitrate rich patches (Remans et al., 2006). Moreover, it was shown that NRT1.1 can transport auxin and that nitrate suppresses this transport (Krouk et al., 2010). In the proposed model, auxin transport through NRT1.1 recycles auxin from the LR tip. Nitrate inhibition leads to auxin accumulation in the tip and thus enhances LR elongation. Conversely, low-N increases auxin recycling and hence slows down LR elongation (Krouk et al., 2010). The recycled auxin may become available for the growth of second-order LRs. The question then arises whether CIPK23-phosphorylated AKT1 promotes auxin recycling from the LR tip and how. Efflux of auxin in its acidic form is a potential target process as it will depend on the membrane potential and hence on AKT1 activity (*akt1* root cells are hyperpolarized; Spalding et al., 1999). This hypothesis should be tested in the future by expressing and analyzing auxin reporters in roots of *akt1* plants.

Opposite Action of AKT1 and NRT2.1 Determines the MR Angle

Roots grown on a two-dimensional surface display a typical MR angle due to skewing of the MR toward one side (Oliva and Dunand, 2007). The exact molecular basis of the skewing phenomenon is not known, but several explanations have been proposed. One possible reason is that epidermal cell file rotation (CFR) leads to the root rolling over the surface as it grows; fixed at the base, the growing root produces an angle if rotation occurs in one direction only (Migliaccio and Piconese, 2001; Yuen et al., 2005). Other scientists argued for CFR-independent differential flank growth as another possible reason for the root angle and reported regulation by ethylene, Suc, and nitrate (Buer et al., 2003). At the subcellular level, the cytoskeleton has been implicated as the reason for changes in CFR (Oliva and Dunand, 2007). Alternatively, the orientation of microtubules could cause root skewing through their role in aligning cell wall deposition (Thitamadee et al., 2002; Sedbrook et al., 2004; Yuen et al., 2005).

We previously reported that the response of MR angle to low-K is genetically stable between *Arabidopsis* ecotypes that differ in the low-K response of other RSA parameters (Kellermeier et al., 2013). It is therefore likely that K-regulation of MR angle differs from that of other RSA parameters. Our mutant analysis revealed an opposing, CIPK23-independent action of AKT1 and NRT2.1 with the former promoting right-skewing and the latter promoting left-skewing (Figures 7C to 7E). The finding raises the question of a potential common signal downstream of AKT1 and NRT2.1. pH is a good candidate; K-influx promotes H^+-efflux through the proton pump (Amtmann et al., 1999), while nitrate influx is accompanied by H^+-influx (Miller et al., 2007). The importance of apoplastic pH for extension growth and cell wall deposition is well documented, and its potential effect on MR angle is further supported by a report that root skewing is ATP dependent and reduced in *aha2* mutants, defective in the major root H^+-ATPase (Haruta and Sussman, 2012).

The effect of *AKT1* knockout on MR angle in control conditions mimicked the effect of low-K, yet the latter was independent of functional AKT1 or NRT2.1, suggesting that the primary signal differs. In this case, membrane hyperpolarization might be the crucial factor since it occurs both in wild-type plants in low-K and in *akt1* mutants in sufficient K (Spalding et al., 1999). Membrane hyperpolarization has been shown to evoke changes in the actin cytoskeleton in mammals (Nin et al., 2009; Chifflet and Hernández, 2012), thus providing a potential link to cellular growth and shape. In summary, MR angle is determined by a membrane-delimited regulatory module that involves AKT1 and NRT2.1 but not CIPK23 or NRT1.1. Our findings highlight the regulation of RSA as an important role of well-known membrane transporters that is independent of their function in mineral nutrition.

Integration of RSA Data with Transcriptome and Ionome

Quantitative phenotyping of RSA across multiple nutritional conditions provided an opportunity to relate the nutrient dependency of RSA to that of other molecular and physiological parameters. The root transcriptome profiling across eight NPK combinations revealed distinct response profiles of individual genes and groups of genes, several of which were significantly correlated with the profiles of MR and LR parameters. Established at an early time point before large differences of RSA were visible the identified lists of nutrient-responsive genes are likely to harbor upstream components of the molecular events that lead to specific root architectures. Furthermore, while many of the genes identified here have been previously shown to respond to individual nutrient deficiencies, their expression profiles across multiple deficiencies provide a much finer distinction and offer opportunities to investigate different branches of a complex nutrient signaling network.

How different root architectures affect the nutrient status of aboveground tissues and vice versa is another important question, which cannot be fully understood if nutrients are investigated in isolation. Our analysis of shoot ion concentrations across multiple combinations of N, P, and K revealed that none of them showed a significant correlation with RSA parameters apart from shoot [Fe], which followed a pattern of additive effects of low P and low N similar to that of TRS and branched zone length. The result highlights the future need to include Fe in the combinatorial analysis of nutrient effects. We did not find a correlation between shoot size (fresh weight) and root size (TRS), which is in accordance with previous studies showing that the shoot/root ratio changes under nutrient deficiency (Hermans et al., 2006). Taking shoot size into account to calculate absolute shoot ion contents per plant, we found a significant positive correlation between LR number and the amount of ions in the shoot, which suggests that the number of LRs is the most important RSA feature determining the overall uptake of ions into the plant. These findings need now to be corroborated by detailed studies relating shoot ion contents and concentrations to root ion contents and concentrations as well as nutrient uptake and root-shoot allocation rates. This was not possible in our study since RSA was measured noninvasively in the same plants over a period of time that exceeded the time points analyzed. However, the shoot ion concentration profiles provide an important reference for the nutrient status of the plants in each condition, which will enable future integration of additional physiological parameters with the detailed RSA data generated here.

METHODS

Plant Material and Growth Conditions

Arabidopsis thaliana Col-0 seeds were used as the wild type. Mutant lines in Col-0 background were obtained from NASC or ABRC: *akt1* (SALK_071803; Rubio et al., 2008), *chl1-5* (N6384; Tsay et al., 1993), *cipk23* (SALK_112091; Ho et al., 2009), *hak5* (SALK_005604; Rubio et al., 2008), and *nrt2.1* (SALK_035429; Little et al., 2005). Homozygosity was verified with primer combinations used in previous studies on the same lines (Tsay et al., 1993; Little et al., 2005; Rubio et al., 2008; Ho et al., 2009).

Growth of *Arabidopsis* seedlings was as described (Kellermeier and Amtmann, 2013). In brief, seeds were surface sterilized and stratified for 3 d in the dark at 4°C. For RSA analysis, five seeds per plate were sown on square agar plates containing 35 mL of growth media. For microarray and ionomic analysis, the number of seedlings per plate was higher and the volume of media was increased accordingly. The top 2 cm of the agar was removed to avoid nutrient leakage into shoots and plates were placed vertically into boxes inside the growth chamber. Seedlings were grown in SDs (9/15 h light/dark) and LDs (16/8 h) at 22/18°C with a light intensity of 160 μmol m^{-2} s^{-1}. For high-light experiments, the light intensity was increased to 280 µmol m^{-2} s^{-1}. All plates were checked for germination 3 d after sowing. Nongerminated seeds were discarded from further analysis.

The macronutrient composition of the growth media is given in Supplemental Table 1. Sufficient/deficient concentrations were 2/0.5 mM nitrate, 0.5/0.2 mM phosphate, 2/0.5 mM potassium, and 0.25/0.025 mM sulfate. All media contained the following micronutrients: 42.5 μM Fe(III) Na-EDTA, 1.8 μM $MnSO_4$, 45 μM H_3BO_3, 0.38 μM $ZnSO_4$, 0.015 μM $(NH_4)_6Mo_7O_{24}$, 0.16 μM $CuSO_4$, and 0.01 μM $CoCl_2$. Media were buffered with 2 mM MES, adjusted to pH 5.6 with Tris-HCl, and supplied with 0.5% Suc and 1% agar. The importance of the agar for RSA phenotyping has been pointed out before (Gruber et al., 2013). All experiments in this study were performed with agar A-1296 (Sigma-Aldrich). The elemental composition of individual agar batches used over the course of the study was tested by ICP-OES and is shown in Supplemental Table 6. The main phenotyping experiment (16 nutrient conditions $\times$ 2 light conditions) was performed with agar batch 030M0005.

Analysis of RSA

Root images were taken using a flatbed scanner (CanoScan 5600F; Canon) at a resolution of 200 dpi at various time points. Images were analyzed with EZ Rhizo software (Armengaud et al., 2009b), and all recorded RSA parameters were stored in a database. LR system size (LRS, in percent of TRS) and mean LR length within the top and second from top quartiles of the MR (LRP 0.25 and LRP 0.50) were calculated as additional parameters for each root. Statistical analyses were performed in XLStat (Addinsoft) and Sigma Plot (version 11.0) based on all measured RSA data (Supplemental Data Set 1). Five-way ANOVA was computed for each RSA parameter separately using daylength, N, P, K, and S as environmental variables (factors) at two levels (high and low). After calculation of the full ANOVA model (type III sum of squares), all nonsignificant effects were eliminated and the model was recalculated. This procedure was repeated until only significant effects remained. SS of each significant factor or interaction was related to the sum of all SS (100%) to obtain a measure of its contribution to the overall variation of the RSA parameter (explained

percentage of variation; colored bars in Figure 1). The cumulative SS of the nonsignificant effects was also expressed as percentage from the total sum of SS (not explained; gray bars in Figure 1). For Figure 2, the same iterative procedure was applied separately for plants grown in different daylengths, using four-way ANOVA with N, P, K, and S as factors. Tukey's *t* test was used for pairwise comparisons of RSA data from plants grown in different media, different daylength, or light conditions (as indicated in the figure legends). For comparison of RSA profiles, the mean of each RSA parameter in a given medium was normalized to the mean of the same parameter measured in the control medium (sufficient NPKS). From these data, radar charts were generated using the radar-chart option in Excel (Supplemental Data Set 3).

Microarray Analysis

Root tissue of seedlings grown for 6 d on vertical agar plates with eight different media (all combinations of sufficient/deficient NPK supply) was collected and frozen in liquid nitrogen. Total RNA was extracted from roots using an RNeasy plant mini kit (Qiagen). Labeling and hybridization of cRNA to the *Arabidopsis* GeneChip ATH1 (Affymetrix) was performed by the Glasgow Polyomics Facility according to Affymetrix protocols. For each nutrient condition, three independently grown batches of plants were analyzed (24 arrays in total). Hybridization signal intensities for each gene were subjected to quality control and normalization using Affymetrix Expression Console (version 1.1) and Partek Genomics Suite (version 6.10.2010). Each treatment (nutrient deficient) sample was compared with the control (fully sufficient) sample. Normalized signal intensities and mean $\log_2$ ratios (treatment/control) are supplied as Excel files (Supplemental Data Set 3). Significant responses across the three replicates were identified by the Rank Product method (Breitling et al., 2004). Nutrient-responsive genes were selected using the following constraints: signal intensity > 100, false discovery rate < 0.001, and fold change > 4 in at least one of the treatments. Mean relative signals of these genes across all treatments were further analyzed with Partek. Hierarchical clustering based on Euclidian distance separated the genes into two main groups (up- or downregulated by nutrient starvation). For each group, k-means clustering was performed based on Pearson correlation of the response profiles. The optimal cluster number out of 20 was determined from the minimal Davies-Bouldin index. Pearson correlation between mean transcript profiles of the clusters and RSA responses across the same nutrient conditions were calculated in Sigma Plot (version 11.0).

ICP-MS Analysis of Shoot Ion Concentrations

Shoot tissue of plants grown in three independent batches was harvested 10 DAG. After determination of fresh weight, shoots were dried for 1 week at 60°C. Concentrated nitric acid (0.7 mL per tube) (trace metal grade; T.J. Baker) with indium internal standard (20 ppb) was added and the samples were digested at 115°C for 5 h using digital dry block heaters inside a fume hood. The acid digested samples were diluted to a final volume of 6 mL with 18 MΩ water. Aliquots were transferred from the digestion tubes into 96-well deepwell plates for analysis. Elemental analysis was performed by ICP-MS using an Elan DRC II (Perkin-Elmer) equipped with Apex sample introduction system and SC-2 autosampler (Elemental Scientific). Twenty elements (Li, B, Na, Mg, P, S, K, Ca, Mn, Fe, Co, Ni, Cu, Zn, As, Se, Rb, Sr, Mo, and Cd) were monitored; their concentrations were obtained using calibration standards with blanks and the external calibration method of the Elan software (version 3.4).

Accession Numbers

Sequence data from this article can be found in the Arabidopsis Genome Initiative or GenBank/EMBL databases under the following accession numbers: AKT1 (AT2G26650), CIPK23 (AT1G30270), HAK5 (AT4G13420), NRT2.1 (AT1G08090), NRT1.1/CHL1 (AT1G12110), RPII (AT4G48850), SULTR1.1 (AT4G08620), and SDI1 (AT5G48850). Accession numbers of nutrient-responsive genes shown in Figure 8 are listed in Supplemental Data Set 5 online. Microarray raw data have been deposited in ArrayExpress.

Supplemental Data

The following materials are available in the online version of this article.

Supplemental Figure 1. Schematic Representation of RSA Parameters.

Supplemental Figure 2. PCA Separates Nutrient Effects on the Basis of RSA.

Supplemental Figure 3. Effects of Low K and Low Nitrate on RSA in Wild-Type and Mutant Plants.

Supplemental Figure 4. Hierarchical Clustering of Root Genes Based on Their Transcriptional Response to Combinations of N, P, and K Starvation.

Supplemental Figure 5. Response Profiles of Root Genes in UP Clusters.

Supplemental Figure 6. Response Profiles of Root Genes in DOWN Clusters.

Supplemental Figure 7. Shoot Micronutrient Concentrations and Fresh Weights of Plants Grown in Different Combinations of N, P, and K.

Supplemental Figure 8. S-Deficiency Indicators in Plants Grown on Low-S Media.

Supplemental Table 1. Nutrient Composition of Growth Media.

Supplemental Table 2. Pearson Correlation Coefficients between All Quantified Root Parameters.

Supplemental Table 3. Contribution of RSA Parameters to Principal Components.

Supplemental Table 4. P Values for Comparisons Shown in Figure 5A: LRP0.25.

Supplemental Table 5. P Values for Comparisons Shown in Figure 5B: Apical.

Supplemental Table 6. Elemental Analysis of Different Batches of Agar Used in This Study.

Supplemental Data Set 1. Raw Data of Quantified Root System Architecture.

Supplemental Data Set 2. P Values and Sum Squares for Results Shown in Figures 1 and 2.

Supplemental Data Set 3. Root Architecture Responses to Individual Combinations of NPKS-Starvation (Radar Graphs).

Supplemental Data Set 4. Absolute and Relative Transcript Levels in Roots across Eight Nutrient Conditions Obtained by Microarray Analysis (All Genes).

Supplemental Data Set 5. Mean Transcriptional Responses of Genes in UP and DOWN Clusters.

ACKNOWLEDGMENTS

We thank Pawel Herzyk and Jing Wang (Glasgow Polyomics Facility) for carrying out the microarray experiments and advising on data analysis. We thank Amparo Ruiz Prado and Mary Ann Madsen for

help with plant growth and RNA isolation. We appreciate funding and fruitful academic support of F.K. from the Gatsby Charitable Foundation (Sainsbury studentship). P.A. was supported by the Biotechnology and Biological Science Research Council and by the Leverhulme Trust.

AUTHOR CONTRIBUTIONS

F.K., P.A., and A.A. designed the experiments. F.K. carried out all the experimental work apart from the transcript analysis of low-S markers (carried out by T.J.S.) and the elemental analysis (carried out by J.D. and D.E.S.). F.K. and A.A. analyzed the data and wrote the article with contributions from all other authors.

Received December 20, 2013; revised March 1, 2014; accepted March 12, 2014; published April 1, 2014.

REFERENCES

Abel, S. (2011). Phosphate sensing in root development. Curr. Opin. Plant Biol. **14:** 303–309.

Al-Ghazi, Y., Muller, B., Pinloche, S., Tranbarger, T.J., Nacry, P., Rossignol, M., Tardieu, F., and Doumas, P. (2003). Temporal responses of Arabidopsis root architecture to phosphate starvation: Evidence for the involvement of auxin signalling. Plant Cell Environ. **26:** 1053–1066.

Alhendawi, R.A., Kirkby, E.A., and Pilbeam, D.J. (2005). Evidence that sulfur deficiency enhances molybdenum transport in xylem sap of tomato plants. J. Plant Nutr. **28:** 1347–1353.

Amtmann, A., and Blatt, M.R. (2009). Regulation of macronutrient transport. New Phytol. **181:** 35–52.

Amtmann, A., Jelitto, T.C., and Sanders, D. (1999). K+-Selective inward-rectifying channels and apoplastic pH in barley roots. Plant Physiol. **120:** 331–338.

Armengaud, P., Sulpice, R., Miller, A.J., Stitt, M., Amtmann, A., and Gibon, Y. (2009a). Multilevel analysis of primary metabolism provides new insights into the role of potassium nutrition for glycolysis and nitrogen assimilation in Arabidopsis roots. Plant Physiol. **150:** 772–785.

Armengaud, P., Zambaux, K., Hills, A., Sulpice, R., Pattison, R.J., Blatt, M.R., and Amtmann, A. (2009b). EZ-Rhizo: Integrated software for the fast and accurate measurement of root system architecture. Plant J. **57:** 945–956.

Breitling, R., Armengaud, P., Amtmann, A., and Herzyk, P. (2004). Rank products: A simple, yet powerful, new method to detect differentially regulated genes in replicated microarray experiments. FEBS Lett. **573:** 83–92.

Buer, C.S., Wasteneys, G.O., and Masle, J. (2003). Ethylene modulates root-wave responses in Arabidopsis. Plant Physiol. **132:** 1085–1096.

Chen, L.Q., Qu, X.Q., Hou, B.H., Sosso, D., Osorio, S., Fernie, A.R., and Frommer, W.B. (2012). Sucrose efflux mediated by SWEET proteins as a key step for phloem transport. Science **335:** 207–211.

Chifflet, S., and Hernández, J.A. (2012). The plasma membrane potential and the organization of the actin cytoskeleton of epithelial cells. Int. J. Cell Biol. **2012:** 121424.

Den Herder, G., Van Isterdael, G., Beeckman, T., and De Smet, I. (2010). The roots of a new green revolution. Trends Plant Sci. **15:** 600–607.

De Smet, I., et al. (2012). Analyzing lateral root development: how to move forward. Plant Cell **24:** 15–20.

Dubrovsky, J.G., and Forde, B.G. (2012). Quantitative analysis of lateral root development: Pitfalls and how to avoid them. Plant Cell **24:** 4–14.

Gan, Y., Bernreiter, A., Filleur, S., Abram, B., and Forde, B.G. (2012). Overexpressing the ANR1 MADS-box gene in transgenic plants provides new insights into its role in the nitrate regulation of root development. Plant Cell Physiol. **53:** 1003–1016.

Giehl, R.F., Meda, A.R., and von Wirén, N. (2009). Moving up, down, and everywhere: Signaling of micronutrients in plants. Curr. Opin. Plant Biol. **12:** 320–327.

Gifford, M.L., Dean, A., Gutierrez, R.A., Coruzzi, G.M., and Birnbaum, K.D. (2008). Cell-specific nitrogen responses mediate developmental plasticity. Proc. Natl. Acad. Sci. USA **105:** 803–808.

Gojon, A., Nacry, P., and Davidian, J.C. (2009). Root uptake regulation: A central process for NPS homeostasis in plants. Curr. Opin. Plant Biol. **12:** 328–338.

Gruber, B.D., Giehl, R.F., Friedel, S., and von Wirén, N. (2013). Plasticity of the Arabidopsis root system under nutrient deficiencies. Plant Physiol. **163:** 161–179.

Gutiérrez, R.A., Lejay, L.V., Dean, A., Chiaromonte, F., Shasha, D.E., and Coruzzi, G.M. (2007). Qualitative network models and genome-wide expression data define carbon/nitrogen-responsive molecular machines in Arabidopsis. Genome Biol. **8:** R7.

Haruta, M., and Sussman, M.R. (2012). The effect of a genetically reduced plasma membrane protonmotive force on vegetative growth of Arabidopsis. Plant Physiol. **158:** 1158–1171.

Hermans, C., Hammond, J.P., White, P.J., and Verbruggen, N. (2006). How do plants respond to nutrient shortage by biomass allocation? Trends Plant Sci. **11:** 610–617.

Hirsch, J., Marin, E., Floriani, M., Chiarenza, S., Richaud, P., Nussaume, L., and Thibaud, M.C. (2006). Phosphate deficiency promotes modification of iron distribution in *Arabidopsis* plants. Biochimie **88:** 1767–1771.

Ho, C.H., Lin, S.H., Hu, H.C., and Tsay, Y.F. (2009). CHL1 functions as a nitrate sensor in plants. Cell **138:** 1184–1194.

Hodge, A., Berta, G., Doussan, C., Merchan, F., and Crespi, M. (2009). Plant root growth, architecture and function. Plant Soil **321:** 153–187.

Howarth, J.R., Parmar, S., Barraclough, P.B., and Hawkesford, M.J. (2009). A sulphur deficiency-induced gene, sdi1, involved in the utilization of stored sulphate pools under sulphur-limiting conditions has potential as a diagnostic indicator of sulphur nutritional status. Plant Biotechnol. J. **7:** 200–209.

Kellermeier, F., and Amtmann, A. (2013). Phenotyping jasmonate regulation of root growth. Methods Mol. Biol. **1011:** 25–32.

Kellermeier, F., Chardon, F., and Amtmann, A. (2013). Natural variation of Arabidopsis root architecture reveals complementing adaptive strategies to potassium starvation. Plant Physiol. **161:** 1421–1432.

Krouk, G., et al. (2010). Nitrate-regulated auxin transport by NRT1.1 defines a mechanism for nutrient sensing in plants. Dev. Cell **18:** 927–937.

Kutschera, U., and Briggs, W.R. (2012). Root phototropism: From dogma to the mechanism of blue light perception. Planta **235:** 443–452.

Li, J.Y., et al. (2010). The Arabidopsis nitrate transporter NRT1.8 functions in nitrate removal from the xylem sap and mediates cadmium tolerance. Plant Cell **22:** 1633–1646.

Li, L., Kim, B.G., Cheong, Y.H., Pandey, G.K., and Luan, S. (2006). A Ca(2)+ signaling pathway regulates a K(+) channel for low-K response in Arabidopsis. Proc. Natl. Acad. Sci. USA **103:** 12625–12630.

Little, D.Y., Rao, H.Y., Oliva, S., Daniel-Vedele, F., Krapp, A., and Malamy, J.E. (2005). The putative high-affinity nitrate transporter

NRT2.1 represses lateral root initiation in response to nutritional cues. Proc. Natl. Acad. Sci. USA **102:** 13693–13698.

López-Bucio, J., Cruz-Ramírez, A., and Herrera-Estrella, L. (2003). The role of nutrient availability in regulating root architecture. Curr. Opin. Plant Biol. **6:** 280–287.

López-Bucio, J., Hernández-Abreu, E., Sánchez-Calderón, L., Nieto-Jacobo, M.F., Simpson, J., and Herrera-Estrella, L. (2002). Phosphate availability alters architecture and causes changes in hormone sensitivity in the Arabidopsis root system. Plant Physiol. **129:** 244–256.

Malamy, J.E., and Ryan, K.S. (2001). Environmental regulation of lateral root initiation in Arabidopsis. Plant Physiol. **127:** 899–909.

Maruyama-Nakashita, A., Nakamura, Y., Yamaya, T., and Takahashi, H. (2004). Regulation of high-affinity sulphate transporters in plants: Towards systematic analysis of sulphur signalling and regulation. J. Exp. Bot. **55:** 1843–1849.

Migliaccio, F., and Piconese, S. (2001). Spiralizations and tropisms in Arabidopsis roots. Trends Plant Sci. **6:** 561–565.

Miller, A.J., Fan, X.R., Orsel, M., Smith, S.J., and Wells, D.M. (2007). Nitrate transport and signalling. J. Exp. Bot. **58:** 2297–2306.

Miura, K., Lee, J., Gong, Q.Q., Ma, S.S., Jin, J.B., Yoo, C.Y., Miura, T., Sato, A., Bohnert, H.J., and Hasegawa, P.M. (2011). SIZ1 regulation of phosphate starvation-induced root architecture remodeling involves the control of auxin accumulation. Plant Physiol. **155:** 1000–1012.

Nacry, P., Canivenc, G., Muller, B., Azmi, A., Van Onckelen, H., Rossignol, M., and Doumas, P. (2005). A role for auxin redistribution in the responses of the root system architecture to phosphate starvation in Arabidopsis. Plant Physiol. **138:** 2061–2074.

Nin, V., Hernández, J.A., and Chifflet, S. (2009). Hyperpolarization of the plasma membrane potential provokes reorganization of the actin cytoskeleton and increases the stability of adherens junctions in bovine corneal endothelial cells in culture. Cell Motil. Cytoskeleton **66:** 1087–1099.

Nunes-Nesi, A., Fernie, A.R., and Stitt, M. (2010). Metabolic and signaling aspects underpinning the regulation of plant carbon nitrogen interactions. Mol. Plant **3:** 973–996.

Oliva, M., and Dunand, C. (2007). Waving and skewing: how gravity and the surface of growth media affect root development in Arabidopsis. New Phytol. **176:** 37–43.

Pérez-Torres, C.A., López-Bucio, J., Cruz-Ramírez, A., Ibarra-Laclette, E., Dharmasiri, S., Estelle, M., and Herrera-Estrella, L. (2008). Phosphate availability alters lateral root development in Arabidopsis by modulating auxin sensitivity via a mechanism involving the TIR1 auxin receptor. Plant Cell **20:** 3258–3272.

Remans, T., Nacry, P., Pervent, M., Filleur, S., Diatloff, E., Mounier, E., Tillard, P., Forde, B.G., and Gojon, A. (2006). The Arabidopsis NRT1.1 transporter participates in the signaling pathway triggering root colonization of nitrate-rich patches. Proc. Natl. Acad. Sci. USA **103:** 19206–19211.

Rosas, U., Cibrian-Jaramillo, A., Ristova, D., Banta, J.A., Gifford, M.L., Fan, A.H., Zhou, R.W., Kim, G.J., Krouk, G., Birnbaum, K.D., Purugganan, M.D., and Coruzzi, G.M. (2013). Integration of responses within and across Arabidopsis natural accessions uncovers loci controlling root systems architecture. Proc. Natl. Acad. Sci. USA **110:** 15133–15138.

Rouached, H., Wirtz, M., Alary, R., Hell, R., Arpat, A.B., Davidian, J.C., Fourcroy, P., and Berthomieu, P. (2008). Differential regulation of the expression of two high-affinity sulfate transporters, SULTR1.1 and SULTR1.2, in Arabidopsis. Plant Physiol. **147:** 897–911.

Rubio, F., Alemán, F., Nieves-Cordones, M., and Martínez, V. (2010). Studies on Arabidopsis athak5, atakt1 double mutants disclose the range of concentrations at which AtHAK5, AtAKT1 and unknown systems mediate K uptake. Physiol. Plant. **139:** 220–228.

Rubio, F., Nieves-Cordones, M., Alemán, F., and Martínez, V. (2008). Relative contribution of AtHAK5 and AtAKT1 to K+ uptake in the high-affinity range of concentrations. Physiol. Plant. **134:** 598–608.

Sedbrook, J.C., Ehrhardt, D.W., Fisher, S.E., Scheible, W.R., and Somerville, C.R. (2004). The Arabidopsis sku6/spiral1 gene encodes a plus end-localized microtubule-interacting protein involved in directional cell expansion. Plant Cell **16:** 1506–1520.

Spalding, E.P., Hirsch, R.E., Lewis, D.R., Qi, Z., Sussman, M.R., and Lewis, B.D. (1999). Potassium uptake supporting plant growth in the absence of AKT1 channel activity: Inhibition by ammonium and stimulation by sodium. J. Gen. Physiol. **113:** 909–918.

Svistoonoff, S., Creff, A., Reymond, M., Sigoillot-Claude, C., Ricaud, L., Blanchet, A., Nussaume, L., and Desnos, T. (2007). Root tip contact with low-phosphate media reprograms plant root architecture. Nat. Genet. **39:** 792–796.

Thitamadee, S., Tuchihara, K., and Hashimoto, T. (2002). Microtubule basis for left-handed helical growth in Arabidopsis. Nature **417:** 193–196.

Ticconi, C.A., Lucero, R.D., Sakhonwasee, S., Adamson, A.W., Creff, A., Nussaume, L., Desnos, T., and Abel, S. (2009). ER-resident proteins PDR2 and LPR1 mediate the developmental response of root meristems to phosphate availability. Proc. Natl. Acad. Sci. USA **106:** 14174–14179.

Tsay, Y.F., Ho, C.H., Chen, H.Y., and Lin, S.H. (2011). Integration of nitrogen and potassium signaling. Annu. Rev. Plant Biol. **62:** 207–226.

Tsay, Y.F., Schroeder, J.I., Feldmann, K.A., and Crawford, N.M. (1993). The herbicide sensitivity gene CHL1 of Arabidopsis encodes a nitrate-inducible nitrate transporter. Cell **72:** 705–713.

Vidal, E.A., Moyano, T.C., Krouk, G., Katari, M.S., Tanurdzic, M., McCombie, W.R., Coruzzi, G.M., and Gutiérrez, R.A. (2013). Integrated RNA-seq and sRNA-seq analysis identifies novel nitrate-responsive genes in *Arabidopsis thaliana* roots. BMC Genomics **14:** 701.

Ward, J.T., Lahner, B., Yakubova, E., Salt, D.E., and Raghothama, K.G. (2008). The effect of iron on the primary root elongation of Arabidopsis during phosphate deficiency. Plant Physiol. **147:** 1181–1191.

Williamson, L.C., Ribrioux, S.P., Fitter, A.H., and Leyser, H.M.O. (2001). Phosphate availability regulates root system architecture in Arabidopsis. Plant Physiol. **126:** 875–882.

Wu, Y., Zhao, Q., Gao, L., Yu, X.M., Fang, P., Oliver, D.J., and Xiang, C.B. (2010). Isolation and characterization of low-sulphur-tolerant mutants of Arabidopsis. J. Exp. Bot. **61:** 3407–3422.

Xu, J., Li, H.D., Chen, L.Q., Wang, Y., Liu, L.L., He, L., and Wu, W.H. (2006). A protein kinase, interacting with two calcineurin B-like proteins, regulates K+ transporter AKT1 in Arabidopsis. Cell **125:** 1347–1360.

Yuen, C.Y.L., Sedbrook, J.C., Perrin, R.M., Carroll, K.L., and Masson, P.H. (2005). Loss-of-function mutations of ROOT HAIR DEFECTIVE3 suppress root waving, skewing, and epidermal cell file rotation in Arabidopsis. Plant Physiol. **138:** 701–714.

Zhang, H.M., and Forde, B.G. (1998). An Arabidopsis MADS box gene that controls nutrient-induced changes in root architecture. Science **279:** 407–409.